

Flavor instabilities in the multi-angle neutrino line model

Sajad Abbar,^{*} Huaiyu Duan,[†] and Shashank Shalgar[‡]

Department of Physics & Astronomy, University of New Mexico, Albuquerque, NM 87131, USA

(Dated: December 15, 2021)

Neutrino flavor oscillations in the presence of ambient neutrinos is nonlinear in nature which leads to interesting phenomenology that has not been well understood. It was recently shown that, in the two-dimensional, two-beam neutrino Line model, the inhomogeneous neutrino oscillation modes on small distance scales can become unstable at larger neutrino densities than the homogeneous mode does. We develop a numerical code to solve neutrino oscillations in the multi-angle/beam Line model with a continuous neutrino angular distribution. We show that the inhomogeneous oscillation modes can occur at even higher neutrino densities in the multi-angle model than in the two-beam model. We also find that the inhomogeneous modes on sufficiently small scales can be unstable at smaller neutrino densities with ambient matter than without, although a larger matter density does shift the instability region of the homogeneous mode to higher neutrino densities in the Line model as it does in the one-dimensional supernova Bulb model. Our results suggest that the inhomogeneous neutrino oscillation modes can be difficult to treat numerically because the problem of spurious oscillations becomes more severe for oscillations on smaller scales.

PACS numbers: 14.60.Pq

I. INTRODUCTION

The observation of neutrino flavor oscillations has established that neutrinos have non-vanishing masses and that their propagation (or mass) eigenstates are linear combinations of weak-interaction states. One of the remarkable successes in the field of experimental particle physics has been the measurement of all neutrino mixing parameters except the sign of the atmospheric mass-squared difference and the \mathcal{CP} violation phase.

Neutrino flavor oscillations can be modified by the potential due to the presence of electrons and nucleons in the medium [1, 2] or the presence of ambient neutrinos [3–5]. There are two major differences in the phenomenology of neutrino flavor oscillations due to the presence of ambient neutrinos as opposed to ordinary matter. Firstly, unlike ordinary matter the presence of ambient neutrinos makes the neutrino flavor evolution nonlinear in nature. Secondly, in the case of ordinary matter the electrons and nucleons are usually non-relativistic, and the potential experienced by neutrinos is independent of direction to a very good approximation (see [6] for a review). This is not true in the case of neutrino-neutrino self-interaction. These two differences make neutrino oscillations in the neutrino medium very interesting and at the same time a challenging problem solve. It has been shown that a dense neutrino gas can undergo flavor oscillations collectively [7, 8].

The effects of neutrino-neutrino interaction can be important in extreme environments with large neutrino densities like that in the interior of a core-collapse supernova. It was discovered in numerical simulations that the neutrino flavor evolution can be dramatically different for the normal and inverted hierarchies inside supernovae [9, 10]. However, in order to make the numerical simulations manageable, a simplified one-dimensional supernova model called the (neutrino) Bulb model was used. There are several effects that are not taken into account in the Bulb model, although they can modify neutrino oscillations significantly. For example, it has been found that the neutrino emission with an (approximate) axial symmetry around the radial direction can evolve into a configuration with a large axial asymmetry [11, 12]. It has also been suggested that the back-scattering of neutrinos from the nucleons in the envelope of the supernova can lead to significant modification of the neutrino potential [13].

In this paper we investigate the physics of collective neutrino oscillations in the neutrino Line model with two spatial dimensions. The study of this model can provide us with useful insights into the qualitative differences of the phenomenology of collective neutrino oscillations in models with one and multiple spatial dimensions. This study is a generalization of the work done for the two-beam Line model in Ref. [14] where only two neutrino beams are emitted from each neutrino source point.

^{*} sabbar@unm.edu

[†] duan@unm.edu

[‡] shashankshalgar@unm.edu

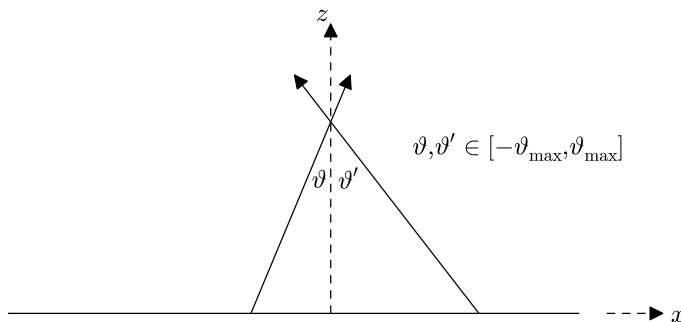


FIG. 1. A schematic diagram of the two dimensional (neutrino) Line model. Each point on the x -axis or the “neutrino Line” emits neutrino beams with emission angles ϑ within range $[-\vartheta_{\max}, \vartheta_{\max}]$.

II. THE NEUTRINO LINE MODEL

A. Equations of motion

In the stationary, two-dimensional (neutrino) Line model neutrinos and antineutrinos are emitted from the x -axis or the “neutrino Line” and propagate in the x - z plane (see Fig. 1). We assume that the neutrinos and antineutrinos are of single energy E and the same normalized angular distribution $g(\vartheta)$ such that the number fluxes of the neutrino and antineutrino within angle range $[\vartheta, \vartheta + d\vartheta]$ are $n_\nu g(\vartheta) d\vartheta$ and $n_{\bar{\nu}} g(\vartheta) d\vartheta$, respectively, where ϑ is the emission angle of the neutrino beam, and n_ν and $n_{\bar{\nu}}$ are the (constant) total number densities of the neutrino and antineutrino, respectively. The flavor quantum states of the neutrino and antineutrino of emission angle ϑ and at position (x, z) are given by density matrices $\rho_\vartheta(x, z)$ and $\bar{\rho}_\vartheta(x, z)$, respectively [15]. We use the normalization condition

$$\text{tr}\rho = \text{tr}\bar{\rho} = 1 \quad (1)$$

such that the diagonal elements of a density matrix give the probabilities for the neutrino or antineutrino to be in the corresponding weak-interaction states. With these conventions the self-interaction potential for $\rho_\vartheta(x, z)$ in the Line model can be written as

$$\mathbf{H}_{\nu\nu, \vartheta}(x, z) = \mu \int [\rho_{\vartheta'}(x, z) - \alpha \bar{\rho}_{\vartheta'}(x, z)] [1 - \cos(\vartheta - \vartheta')] g(\vartheta') d\vartheta', \quad (2)$$

where $\mu = \sqrt{2}G_F n_\nu$ with G_F being the Fermi coupling constant, and $\alpha = n_{\bar{\nu}}/n_\nu$. In the Line model the strength of the neutrino self-interaction μ is constant. In realistic astrophysical environments such as core-collapse supernovae, however, μ can decrease with increasing distance from the neutrino source.

The flavor evolution of the neutrino or antineutrino is governed by the equation of motion (EoM)

$$i\mathbf{v}_\vartheta \cdot \nabla \rho_\vartheta = [\mathbf{H}_{\text{vac}} + \mathbf{H}_{\text{mat}} + \mathbf{H}_{\nu\nu, \vartheta}, \rho_\vartheta], \quad (3)$$

where \mathbf{v}_ϑ is the unit vector that denotes the propagation direction of the neutrino with emission angle ϑ , and \mathbf{H}_{vac} and \mathbf{H}_{mat} are the standard vacuum mixing Hamiltonian and matter potential, respectively. In this work we assume the mixing between two active neutrino flavors ν_e and ν_τ with small vacuum mixing angle $\theta_v \ll 1$. Therefore,

$$\mathbf{H}_\omega = \mathbf{H}_{\text{vac}} + \mathbf{H}_{\text{mat}} \approx \frac{(\lambda - \eta\omega)}{2} \begin{pmatrix} 1 & 0 \\ 0 & -1 \end{pmatrix} = \frac{(\lambda - \eta\omega)}{2} \sigma_3, \quad (4)$$

where $\lambda = \sqrt{2}G_F n_e$ with n_e being the net electron number density, η is a parameter which takes a value of either $+1$ or -1 for the normal neutrino mass hierarchy (NH, the mass-squared difference $\Delta m^2 > 0$) or the inverted hierarchy (IH, $\Delta m^2 < 0$), and $\omega = |\Delta m^2|/2E$ is the vacuum oscillation frequency of the neutrino. Eq. (3) can also be written in a more explicit form:

$$i(\cos \vartheta \partial_z + \sin \vartheta \partial_x) \rho_\vartheta = \frac{(\lambda - \eta\omega)}{2} [\sigma_3, \rho_\vartheta] + \mu \int [1 - \cos(\vartheta - \vartheta')] [\rho_{\vartheta'} - \alpha \bar{\rho}_{\vartheta'}, \rho_\vartheta] g(\vartheta') d\vartheta'. \quad (5)$$

The EoM for $\bar{\rho}_\vartheta$ is the same as Eq. (5) except with replacement $\omega \rightarrow -\omega$.

As in Ref. [14] we impose a periodic boundary condition along the x axis such that $\rho_\vartheta(x+L, z) = \rho_\vartheta(x, z)$ and $\bar{\rho}_\vartheta(x+L, z) = \bar{\rho}_\vartheta(x, z)$. It is convenient to recast the x -dependence of the neutrino density matrix in terms of Fourier moments:

$$\rho_{m,\vartheta}(z) = \frac{1}{L} \int_0^L e^{-ik_m x} \rho_\vartheta(x, z) dx, \quad \bar{\rho}_{m,\vartheta}(z) = \frac{1}{L} \int_0^L e^{-ik_m x} \bar{\rho}_\vartheta(x, z) dx, \quad (6)$$

where $k_m = 2\pi m/L$. It is straightforward to derive the EoM in the moment basis which are

$$\begin{aligned} i \cos \vartheta \partial_z \rho_{m,\vartheta} &= k_m \sin \vartheta \rho_{m,\vartheta} + \frac{(\lambda - \eta\omega)}{2} [\sigma_3, \rho_{m,\vartheta}] \\ &+ \mu \sum_{m'} \int [\rho_{m',\vartheta'} - \alpha \bar{\rho}_{m',\vartheta'}, \rho_{m-m',\vartheta}] [1 - \cos(\vartheta - \vartheta')] g(\vartheta') d\vartheta', \end{aligned} \quad (7a)$$

$$\begin{aligned} i \cos \vartheta \partial_z \bar{\rho}_{m,\vartheta} &= k_m \sin \vartheta \bar{\rho}_{m,\vartheta} + \frac{(\lambda + \eta\omega)}{2} [\sigma_3, \bar{\rho}_{m,\vartheta}] \\ &+ \mu \sum_{m'} \int [\rho_{m',\vartheta'} - \alpha \bar{\rho}_{m',\vartheta'}, \bar{\rho}_{m-m',\vartheta}] [1 - \cos(\vartheta - \vartheta')] g(\vartheta') d\vartheta'. \end{aligned} \quad (7b)$$

B. Collective modes in the linear regime

We assume that the neutrinos and antineutrinos are emitted from the Line source in the electron flavor only. In the regime where neutrino oscillations are insignificant, the neutrino density matrices have the form

$$\rho_\vartheta(x, z) \approx \begin{pmatrix} 1 & \epsilon_\vartheta \\ \epsilon_\vartheta^* & 0 \end{pmatrix}, \quad \bar{\rho}_\vartheta(x, z) \approx \begin{pmatrix} 1 & \bar{\epsilon}_\vartheta \\ \bar{\epsilon}_\vartheta^* & 0 \end{pmatrix}. \quad (8)$$

When there is a flavor instability, the off-diagonal elements of the density matrices grow exponentially, which can result in collective neutrino oscillations. In this section we apply the method of flavor stability analysis to the multi-angle Line model which was first developed in Ref. [16].

In the moment basis we have

$$\rho_{m,\vartheta}(z) \approx \begin{pmatrix} \delta_{0,m} & \epsilon_{m,\vartheta} \\ \epsilon_{-m,\vartheta}^* & 0 \end{pmatrix}, \quad \bar{\rho}_{m,\vartheta}(z) \approx \begin{pmatrix} \delta_{0,m} & \bar{\epsilon}_{m,\vartheta} \\ \bar{\epsilon}_{-m,\vartheta}^* & 0 \end{pmatrix} \quad (9)$$

Keeping only the terms up to $\mathcal{O}(\epsilon)$ in Eq. (7) we obtain

$$i \cos \vartheta \partial_z \epsilon_{m,\vartheta} = [k_m \sin \vartheta + \lambda - \omega\eta + (1 - \alpha)\tilde{\mu}_\vartheta] \epsilon_{m,\vartheta} - \mu \int [1 - \cos(\vartheta - \vartheta')] (\epsilon_{m,\vartheta'} - \alpha \bar{\epsilon}_{m,\vartheta'}) g(\vartheta') d\vartheta', \quad (10a)$$

$$i \cos \vartheta \partial_z \bar{\epsilon}_{m,\vartheta} = [k_m \sin \vartheta + \lambda + \omega\eta + (1 - \alpha)\tilde{\mu}_\vartheta] \bar{\epsilon}_{m,\vartheta} - \mu \int [1 - \cos(\vartheta - \vartheta')] (\epsilon_{m,\vartheta'} - \alpha \bar{\epsilon}_{m,\vartheta'}) g(\vartheta') d\vartheta', \quad (10b)$$

where

$$\tilde{\mu}_\vartheta = \mu \int [1 - \cos(\vartheta - \vartheta')] g(\vartheta') d\vartheta' \quad (11)$$

is the effective strength of neutrino self-interaction for the neutrino beam with emission angle ϑ . As in the two-beam model, the flavor evolution of the neutrino fluxes in different moments is decoupled in the linear regime, although the evolution of the neutrino moments with different emission angles ϑ are still coupled.

Assuming that the m th neutrino moment oscillates with collective oscillation frequency Ω_m , we can write

$$\epsilon_{m,\vartheta}(z) = Q_{m,\vartheta} e^{-i\Omega_m z}, \quad \bar{\epsilon}_{m,\vartheta}(z) = \bar{Q}_{m,\vartheta} e^{-i\Omega_m z}, \quad (12)$$

where $Q_{m,\vartheta}$ and $\bar{Q}_{m,\vartheta}$ are z -independent. Applying this ansatz to Eq. (10) we obtain

$$D_m(\omega, \vartheta) Q_{m,\vartheta} = (a_m - c_m \cos \vartheta - s_m \sin \vartheta) \mu, \quad (13a)$$

$$D_m(-\omega, \vartheta) \bar{Q}_{m,\vartheta} = (a_m - c_m \cos \vartheta - s_m \sin \vartheta) \mu \quad (13b)$$

or

$$Q_{m,\vartheta} = \frac{(a_m - c_m \cos \vartheta - s_m \sin \vartheta)\mu}{D_m(\omega, \vartheta)}, \quad (14a)$$

$$\bar{Q}_{m,\vartheta} = \frac{(a_m - c_m \cos \vartheta - s_m \sin \vartheta)\mu}{D_m(-\omega, \vartheta)}, \quad (14b)$$

where

$$D_m(\pm\omega, \vartheta) = -\Omega \cos \vartheta + k_m \sin \vartheta + \lambda \mp \omega \eta + (1 - \alpha)\tilde{\mu}\vartheta, \quad (15)$$

and

$$a_m = \int (Q_{m,\vartheta'} - \alpha \bar{Q}_{m,\vartheta'}) g(\vartheta') d\vartheta', \quad (16a)$$

$$c_m = \int (Q_{m,\vartheta'} - \alpha \bar{Q}_{m,\vartheta'}) \cos \vartheta' g(\vartheta') d\vartheta', \quad (16b)$$

$$s_m = \int (Q_{m,\vartheta'} - \alpha \bar{Q}_{m,\vartheta'}) \sin \vartheta' g(\vartheta') d\vartheta'. \quad (16c)$$

Substituting Eq. (14) in Eq. (16) we obtain a characteristic equation for (a_m, c_m, s_m) :

$$\begin{pmatrix} I_m[1] - 1 & -I_m[\cos \vartheta] & -I_m[\sin \vartheta] \\ I_m[\cos \vartheta] & -I_m[\cos^2 \vartheta] - 1 & -I_m[\cos \vartheta \sin \vartheta] \\ I_m[\sin \vartheta] & -I_m[\cos \vartheta \sin \vartheta] & -I_m[\sin^2 \vartheta] - 1 \end{pmatrix} \begin{pmatrix} a_m \\ c_m \\ s_m \end{pmatrix} = 0, \quad (17)$$

where

$$I_m[f(\vartheta)] = \int f(\vartheta) g(\vartheta) \left[\frac{\mu}{D_m(\omega, \vartheta)} - \frac{\alpha\mu}{D_m(-\omega, \vartheta)} \right] d\vartheta \quad (18)$$

for arbitrary function $f(\vartheta)$. Eq. (17) holds only when

$$\det \begin{vmatrix} I_m[1] - 1 & -I_m[\cos \vartheta] & -I_m[\sin \vartheta] \\ I_m[\cos \vartheta] & -I_m[\cos^2 \vartheta] - 1 & -I_m[\cos \vartheta \sin \vartheta] \\ I_m[\sin \vartheta] & -I_m[\cos \vartheta \sin \vartheta] & -I_m[\sin^2 \vartheta] - 1 \end{vmatrix} = 0. \quad (19)$$

For given m , λ and μ one can find a set of $\Omega_m^{(i)}(\lambda, \mu)$ ($i = 1, 2, \dots$) which satisfy Eq. (19) and which are the frequencies of the corresponding normal modes of collective neutrino oscillations. When

$$\kappa_m^{(i)} = \text{Im}(\Omega_m^{(i)}) \quad (20)$$

is positive, the corresponding normal mode is unstable and its amplitude grows exponentially. If there exist multiple unstable modes, the mode with the largest exponential growth rate,

$$\kappa_m^{\max} = \max(\kappa_m^{(i)}), \quad (21)$$

will eventually dominate.

III. RESULTS IN THE LINEAR REGIME

A. Numerical computation

We develop a computer code to solve Eq. (7) numerically. In this code the continuous range of ϑ is represented as N discrete angle bins with central value ϑ_i ($i = 1, \dots, N$) and equal interval $\Delta\vartheta$. For an arbitrary function $f(\vartheta)$ one has

$$\int f(\vartheta) d\vartheta \longrightarrow \Delta\vartheta \sum_{i=1}^N f(\vartheta_i). \quad (22)$$

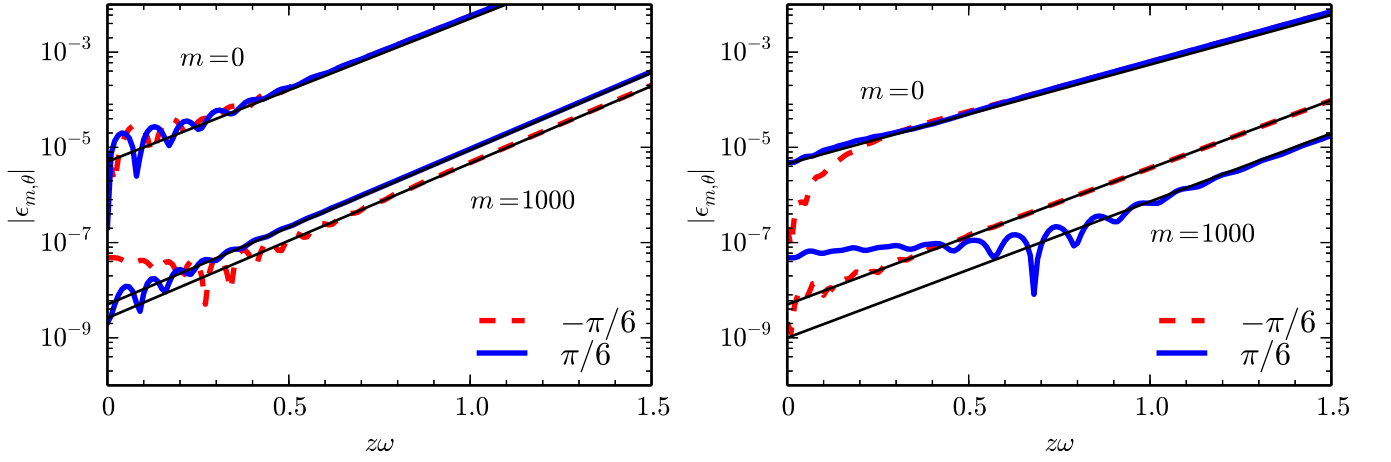


FIG. 2. The evolution of $|\epsilon_{m,\vartheta}|$, the amplitudes of the off-diagonal elements of the neutrino moment matrices $\rho_{m,\vartheta}(z)$, in terms of propagation distance z for the inverted (left) and normal (right) neutrino mass hierarchies. The thick curves represent the numerical solution to Eq. (7) with 0th and 1000th moments only. The thin solid lines represent the exponential growth functions $\sim \exp(\kappa_m^{\max} z)$ predicted by the linear stability analysis. In these calculations we used the parameters listed in Eq. (24), and we took the matter potential $\lambda = 0$ and neutrino potential $\mu/\omega = 1500$ (left) and 3000 (right) which is measured in the vacuum neutrino oscillation frequency ω .

In this work we focus on the neutrino oscillations in the linear regime and the cases with a simple angular distribution which has isotropic neutrino fluxes within range $[-\vartheta_{\max}, \vartheta_{\max}]$, i.e.

$$g(\vartheta) = \begin{cases} \frac{1}{2}\vartheta_{\max}^{-1} & \text{if } \vartheta \in [-\vartheta_{\max}, \vartheta_{\max}], \\ 0 & \text{otherwise.} \end{cases} \quad (23)$$

We choose to present our results with the following parameters

$$\vartheta_{\max} = \pi/6, \quad \alpha = 0.8 \quad \text{and} \quad L = 40\pi\omega^{-1}. \quad (24)$$

Because the evolution of different neutrino moments is decoupled in the linear regime, it is sufficient to include only the 0th and m th moments in studying the evolution of the m th moment in this regime. [The 0th moment is needed because it has large diagonal elements even in the linear regime. See Eq. (9).]

In Fig. 2 we show the numerical solutions to Eq. (7) in two calculations with all but the 0th and 1000th moments being zero. In both calculations, $|\epsilon_{m,\vartheta}|$, the amplitudes of the off-diagonal elements of $\rho_{m,\vartheta}$, grow exponentially which is understood as flavor instabilities. As comparison we plot in Fig. 2 the exponential growth functions $\sim \exp(\kappa_m^{\max} z)$ predicted by the flavor stability analysis, and they agree with the numerical results very well. As a further confirmation, we have compared the shapes of $|Q_{m,\vartheta}|$ and $|\bar{Q}_{m,\vartheta}|$ obtained from flavor stability analysis (the dotted and dashed curves in Fig. 3) with those of $|\epsilon_{m,\vartheta}|$ and $|\bar{\epsilon}_{m,\vartheta}|$ in numerical calculations (not shown), and they also have good agreement. However, to achieve numerical convergence a large number of angle bins may be needed for the following reason.

As pointed out in Ref. [17], there can exist many spurious flavor instabilities in the numerical implementation using the discrete (angle-bin) scheme. This can be seen from the discretized version of Eq. (10):

$$i \cos \vartheta_i \partial_z \epsilon_{m,\vartheta_i} = [k_m \sin \vartheta_i + \lambda - \omega \eta + (1 - \alpha) \tilde{\mu}_{\vartheta_i}] \epsilon_{m,\vartheta_i} - \mu \Delta \vartheta \sum_j [1 - \cos(\vartheta_i - \vartheta_j)] (\epsilon_{m,\vartheta_j} - \alpha \bar{\epsilon}_{m,\vartheta_j}) g(\vartheta_j), \quad (25a)$$

$$i \cos \vartheta_i \partial_z \bar{\epsilon}_{m,\vartheta_i} = [k_m \sin \vartheta_i + \lambda + \omega \eta + (1 - \alpha) \tilde{\mu}_{\vartheta_i}] \bar{\epsilon}_{m,\vartheta_i} - \mu \Delta \vartheta \sum_j [1 - \cos(\vartheta_i - \vartheta_j)] (\epsilon_{m,\vartheta_j} - \alpha \bar{\epsilon}_{m,\vartheta_j}) g(\vartheta_j), \quad (25b)$$

or

$$i \partial_z \epsilon_m = \Lambda_m \cdot \epsilon_m, \quad (26)$$

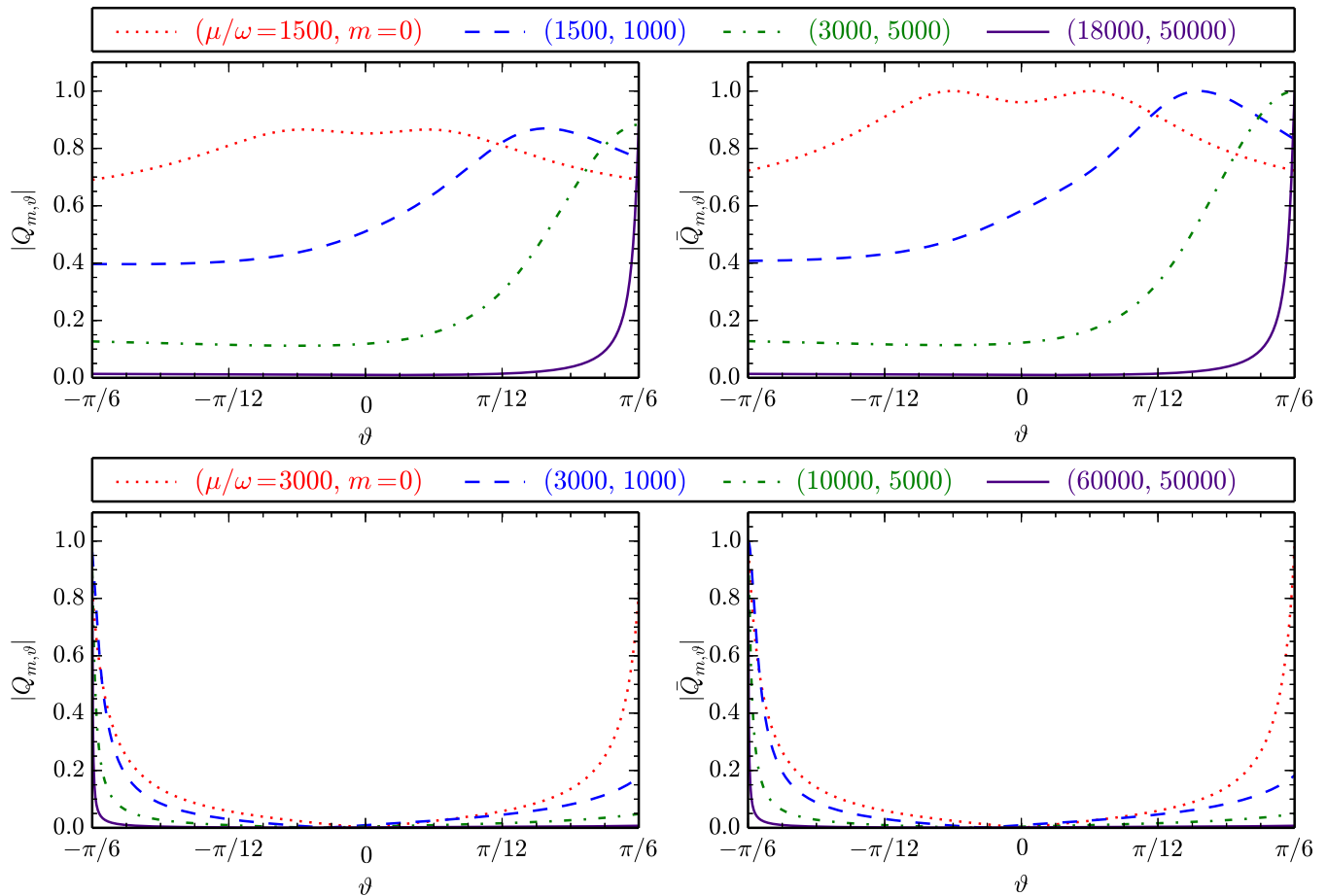


FIG. 3. The amplitudes of the unstable modes of the m th neutrino moments (in arbitrary scale) as functions of neutrino emission angle ϑ which have the largest exponential growth rates in the linear regime at given neutrino number densities (indicated by $\mu = \sqrt{2}G_F n_\nu$ which is measured in the vacuum neutrino oscillation frequency ω). The top and bottom panels are for the inverted and normal neutrino mass hierarchies, respectively. In these calculations we used the parameters listed in Eq. (24), and we took the matter potential $\lambda = 0$.

where $\epsilon_m = (\epsilon_{m,\vartheta_1}, \bar{\epsilon}_{m,\vartheta_1}, \epsilon_{m,\vartheta_2}, \bar{\epsilon}_{m,\vartheta_2}, \dots, \epsilon_{m,\vartheta_N}, \bar{\epsilon}_{m,\vartheta_N})^T$ is a $2N$ -dimensional vector, and Λ_m is a $2N \times 2N$ real matrix. Matrix Λ_m has $2N$ eigenvalues $\Omega_m^{(i)}$ ($i = 1, 2, \dots, 2N$) each of which corresponds to the collective oscillation frequency of a collective mode in the discrete scheme. Many of these collective modes can be unstable, i.e. with $\kappa_m^{(i)} = \text{Im}(\Omega_m^{(i)}) > 0$. Only a few of the unstable modes correspond to the physical instabilities in the continuum limit (of the ϑ distribution), and the rest of them are “spurious” or the artifact of the numerical implementation.

In Fig. 4 we plot the exponential growth rates $\kappa_m^{(i)}$ of all the unstable collective modes both in the discrete scheme and in the continuum limit for the 0th and 5000th moments, respectively. This figure shows that spurious instabilities (in the discrete scheme) can dominate the physical instabilities (in the continuum limit) on small distance scales and/or large neutrino number densities (i.e. large $|m|$ and/or μ). In some extreme cases, e.g., the bottom middle panel of Fig. 4 where $\eta = +1$, $m = 5000$ and $N = 100$, none of the collective modes in the discrete scheme matches the ones in the continuum limit. This is likely due to the fact that $Q_{m,\vartheta}$ and $\bar{Q}_{m,\vartheta}$ become sharply peaked functions of ϑ at large $|m|$ and/or μ , which requires more angle bins to resolve (see Fig. 3). Indeed, the comparison between the middle and right panels of Fig. 4 show that the spurious instabilities are more suppressed when more angle bins are employed.

B. Flavor instabilities and matter effect

We have solved the flavor instabilities of the multi-angle Line model using the angular distribution in Eq. (23) and the parameters listed in Eq. (24). The results for the neutrino gas in the absence of matter are shown in the upper

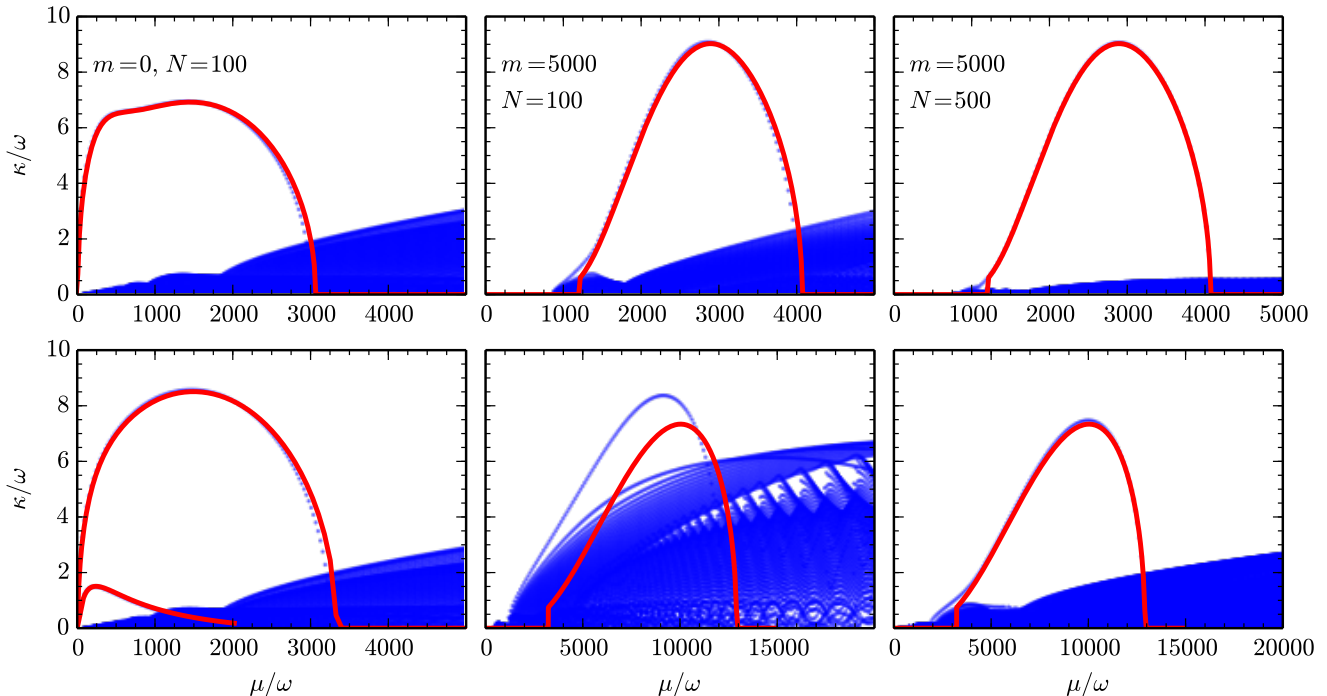


FIG. 4. The exponential growth rates $\kappa_m^{(i)}$ of the unstable collective modes of the m th neutrino moment as functions of neutrino self-interaction strength $\mu = \sqrt{2}G_F n_\nu$ in the discrete angle-bin scheme with N angle bins (as labeled and shown as the dotted curves) and in the continuum limit of angular distribution (solid curves), respectively. Both κ and μ are measured in the vacuum neutrino oscillation frequency ω . The top and bottom panels are for the inverted and normal neutrino mass hierarchies, respectively. In these calculations we used the parameters listed in Eq. (24), and we took the matter potential $\lambda = 0$.

panels of Fig. 5. From this figure one can see that, unlike the two-beam Line model [14], the flavor instabilities in the multi-angle model depends on the neutrino mass hierarchy, and collective oscillations can begin at larger neutrino density in NH than in IH. One also sees that both μ_m^{\max} and μ_m^{\min} , the maximum and minimum μ values where the m th modes are unstable, seem to increase linearly with $|m|$. In contrast, both μ_m^{\max} and μ_m^{\min} increase linearly with $\sqrt{|m|}$ in the two-beam model.¹ This implies that, for sufficiently large $|m|$, flavor instabilities can develop at even larger neutrino densities in the multi-angle model than in the two-beam model.

Unlike in the two-beam model, the presence of matter can affect collective oscillations in the multi-angle model because the neutrinos propagate in different directions can travel through different distances between two lines that are parallel to the neutrino Line. In the lower panels of Fig. 5 we show the flavor instabilities in the multi-angle Line model with $\lambda = 200\omega$. Similar to the situation in the spherical neutrino Bulb model for supernova [16, 18], both μ_m^{\max} and μ_m^{\min} of the homogeneous mode (i.e. with $m = 0$) shift to larger values in the presence of a large matter density in both NH and IH. However, μ_m^{\min} of inhomogeneous modes actually shifts to smaller values for both NH and IH when $|m|$ is sufficiently large.

IV. DISCUSSION

We have used both the numerical method and the linear stability analysis to investigate collective neutrino oscillations in the multi-angle Line model in the linear regime where the neutrino flavor transformation is still small. Although the Line model does not represent any real physical environment, the study of this toy model can provide insights into the important differences between the models of one spatial dimension (e.g. the neutrino Bulb model for supernova) and multi-dimension models.

¹ The definition of neutrino self-coupling strength μ in [14] has taken into account of the geometric factor $1 - \cos(\vartheta - \vartheta')$ and is equivalent to $\tilde{\mu}_\vartheta$ in this paper. For the angular distribution in Eq. (23) $\tilde{\mu}_0 = (1 - \sin \vartheta_{\max}/\vartheta_{\max})\mu \approx 0.045\mu$.

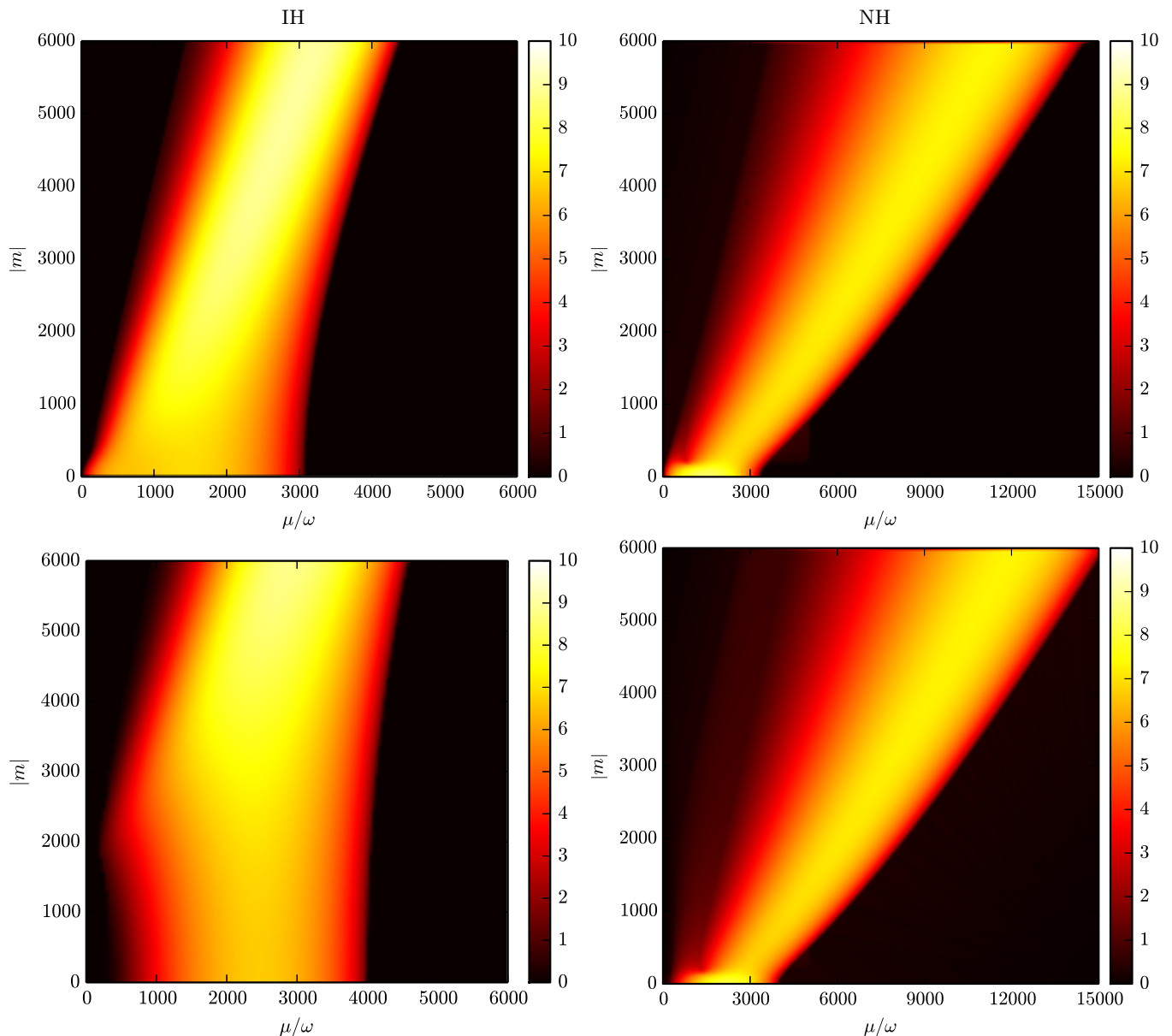


FIG. 5. Maximum exponential growth rate $\kappa_m^{\max}(\lambda, \mu)$ (indicated by the color scale) of the neutrino collective oscillation modes in the multi-angle Line model as a function of moment index m and the neutrino self-coupling strength $\mu = \sqrt{2}G_F n_\nu$. Both κ and μ are measured in the vacuum neutrino oscillation frequency ω . The left and right panels are for the inverted and normal neutrino mass hierarchies, respectively, and the top and bottom panels are for $\lambda = \sqrt{2}G_F n_e = 0$ and 200ω , respectively. In these calculations we assume isotropic neutrino fluxes within angular range $\vartheta \in [-\pi/6, \pi/6]$, and we used the parameters listed in Eq. (24).

An important goal of this work is to check if the inhomogeneous collective modes are suppressed in the multi-angle environment because of the high neutrino densities which is known to exist in the Bulb model [18, 19]. Somewhat surprisingly, our work suggests that, in the absence of ordinary matter, inhomogeneous collective modes on small scales are not only not suppressed in the multi-angle environment, but can become unstable at larger neutrino densities than in the two-beam model.

We also examined whether the presence of a large matter density can suppress collective oscillations in the two-dimensional Line model as in the one-dimensional Bulb model [18]. Our study shows that the presence of ambient matter does suppress inhomogeneous oscillation modes on large distance scales in the Line model as it occurs to the homogeneous modes in the Bulb model. However, it appears that the inhomogeneous modes on very small scales can occur at smaller neutrino number densities with ambient matter than without. In addition, the flavor unstable

region of the certain inhomogeneous modes can extend to the regime of lower neutrino densities than that for the homogeneous mode.

We have shown that, as in the Bulb model, there exist spurious oscillations in the numerical implementation of the multi-angle Line model if the discrete angle-bin scheme is employed. The problem of spurious oscillations appear to be more severe at higher neutrino densities and on smaller distance scales. Although this problem can be mitigated by using more angle bins, it does add complications to the already challenging task of computing collective neutrino oscillations near astrophysical neutrino sources such as core-collapse supernovae and black-hole accretion discs. It is probably helpful to develop the multipole expansion method similar to that for the Bulb model [20].

Our work has focused on the neutrino flavor instabilities in the linear regime. However, not every flavor instability in the linear regime can result in significant neutrino flavor transformation. For example, in the realistic supernova environment, the neutrino density decreases as neutrinos travel away from the center of the supernova which results in the shift of the instability region. It is, therefore, possible that a collective oscillation mode does not grow all the way to the nonlinear regime during the finite distance interval where it is unstable. We have considered the mixing of two neutrino flavors only, which can be quite different from the neutrino flavor transformation of three flavors [21]. Ultimately, the phenomenon of collective neutrino oscillations has to be studied in realistic, multi-dimensional models for compact objects such as core-collapse supernovae and black-hole accretion discs before one can fully understand the impact of neutrino oscillations to these extreme environments.

ACKNOWLEDGMENTS

We thank V. Noormofidi and L. Ma for useful discussions. We also appreciate the hospitality of INT/UW where part of this work was done. This work was supported by DOE EPSCoR grant #DE-SC0008142 at UNM.

-
- [1] S. Mikheev and A. Y. Smirnov, *Sov.J.Nucl.Phys.* **42**, 913 (1985).
 - [2] L. Wolfenstein, *Phys.Rev.* **D17**, 2369 (1978).
 - [3] G. M. Fuller, R. W. Mayle, J. R. Wilson, and D. N. Schramm, *Astrophys. J.* **322**, 795 (1987).
 - [4] D. Notzold and G. Raffelt, *Nucl. Phys.* **B307**, 924 (1988).
 - [5] J. T. Pantaleone, *Phys.Lett.* **B287**, 128 (1992).
 - [6] R. Mohapatra and P. Pal, *World Sci.Lect.Notes Phys.* **41**, 1 (1991).
 - [7] V. A. Kostelecky and S. Samuel, *Phys.Lett.* **B318**, 127 (1993).
 - [8] V. A. Kostelecky, J. T. Pantaleone, and S. Samuel, *Phys.Lett.* **B315**, 46 (1993).
 - [9] H. Duan, G. M. Fuller, J. Carlson, and Y.-Z. Qian, *Phys.Rev.Lett.* **97**, 241101 (2006), astro-ph/0608050.
 - [10] H. Duan, G. M. Fuller, J. Carlson, and Y.-Z. Qian, *Phys.Rev.* **D74**, 105014 (2006), astro-ph/0606616.
 - [11] G. Raffelt, S. Sarikas, and D. de Sousa Seixas, *Phys.Rev.Lett.* **111**, 091101 (2013), 1305.7140.
 - [12] A. Mirizzi, *Phys.Rev.* **D88**, 073004 (2013), 1308.1402.
 - [13] J. F. Cherry, J. Carlson, A. Friedland, G. M. Fuller, and A. Vlasenko, *Phys.Rev.Lett.* **108**, 261104 (2012), 1203.1607.
 - [14] H. Duan and S. Shalgar, *Phys.Lett.* **B747**, 139 (2015), 1412.7097.
 - [15] G. Sigl and G. Raffelt, *Nucl.Phys.* **B406**, 423 (1993).
 - [16] A. Banerjee, A. Dighe, and G. Raffelt, *Phys.Rev.* **D84**, 053013 (2011), 1107.2308.
 - [17] S. Sarikas, D. d. S. Seixas, and G. Raffelt, *Phys.Rev.* **D86**, 125020 (2012), 1210.4557.
 - [18] A. Esteban-Pretel, A. Mirizzi, S. Pastor, R. Tomas, G. Raffelt, et al., *Phys.Rev.* **D78**, 085012 (2008), 0807.0659.
 - [19] H. Duan and A. Friedland, *Phys.Rev.Lett.* **106**, 091101 (2011), 1006.2359.
 - [20] H. Duan and S. Shalgar, *JCAP* **1410**, 084 (2014), 1407.7861.
 - [21] A. Friedland, *Phys.Rev.Lett.* **104**, 191102 (2010), 1001.0996.